Inhalation Toxicology

http://informahealthcare.com/iht
ISSN: 0895-8378 (print), 1091-7691 (electronic)

Inhal Toxicol, 2015; 27(4): 207–223
 DOI: 10.3109/08958378.2015.1026620

informa healthcare

RESEARCH ARTICLE

Size effects of single-walled carbon nanotubes on *in vivo* and *in vitro* pulmonary toxicity

Katsuhide Fujita[1,2], Makiko Fukuda[2], Shigehisa Endoh[2], Junko Maru[2], Haruhisa Kato[2,3], Ayako Nakamura[3], Naohide Shinohara[1,2], Kanako Uchino[2], and Kazumasa Honda[1,2]

[1]*Research Institute of Science for Safety and Sustainability (RISS), National Institute of Advanced Industrial Science and Technology (AIST), Tsukuba, Ibaraki, Japan,* [2]*Technology Research Association for Single Wall Carbon Nanotubes (TASC), Tsukuba, Ibaraki, Japan, and* [3]*National Metrology Institute of Japan (NMIJ), National Institute of Advanced Industrial Science and Technology (AIST), Tsukuba, Ibaraki, Japan*

Abstract

To elucidate the effect of size on the pulmonary toxicity of single-wall carbon nanotubes (SWCNTs), we prepared two types of dispersed SWCNTs, namely relatively thin bundles with short linear shapes (CNT-1) and thick bundles with long linear shapes (CNT-2), and conducted rat intratracheal instillation tests and *in vitro* cell-based assays using NR8383 rat alveolar macrophages. Total protein levels, MIP-1α expression, cell counts in BALF, and histopathological examinations revealed that CNT-1 caused pulmonary inflammation and slower recovery and that CNT-2 elicited acute lung inflammation shortly after their instillation. Comprehensive gene expression analysis confirmed that CNT-1-induced genes were strongly associated with inflammatory responses, cell proliferation, and immune system processes at 7 or 30 d post-instillation. Numerous genes were significantly upregulated or downregulated by CNT-2 at 1 d post-instillation. *In vitro* assays demonstrated that CNT-1 and CNT-2 SWCNTs were phagocytized by NR8383 cells. CNT-2 treatment induced cell growth inhibition, reactive oxygen species production, MIP-1α expression, and several genes involved in response to stimulus, whereas CNT-1 treatment did not exert a significant impact in these regards. These results suggest that SWCNTs formed as relatively thin bundles with short linear shapes elicited delayed pulmonary inflammation with slower recovery. In contrast, SWCNTs with a relatively thick bundle and long linear shapes sensitively induced cellular responses in alveolar macrophages and elicited acute lung inflammation shortly after inhalation. We conclude that the pulmonary toxicity of SWCNTs is closely associated with the size of the bundles. These physical parameters are useful for risk assessment and management of SWCNTs.

Keywords

Alveolar macrophages, gene expression profiles, intratracheal instillation, *in vivo*, *in vitro*, single-wall carbon nanotubes

History

Received 16 January 2015
Revised 4 February 2015
Accepted 2 March 2015
Published online 13 April 2015

Introduction

Concerns over the influence of manufactured nanomaterials on human health have parallel developments in nanotechnology. One concern is that while carbon nanotubes (CNTs) will potentially be used in a wide range of industrial products, little is known regarding their potential toxicities. A safety assessment of CNTs in the beginning stages of research and development processes will provide improved risk assessment and management in the workplace.

Address for correspondence: Katsuhide Fujita, Research Institute of Science for Safety and Sustainability, National Institute of Advanced Industrial Science and Technology, Tsukuba, Ibaraki 305-8569, Japan. Tel: +81 298 861 8006. Fax: +81 298 861 8415. E-mail: ka-fujita@aist.go.jp

The fiber pathogenicity paradigm is characterized by robust structure/toxicity relationships that enable the prediction of fiber pathogenicity depending on their length, thickness, and biopersistence (Donaldson et al., 2010). Although it is debatable whether this paradigm is applicable to CNTs, the relationships between the physical properties of CNTs and their toxicity have been discussed (Donaldson et al., 2013). One research team provided evidence that long fibrous MWCNTs show a similar, or even greater, tendency to produce inflammation and fibrosis in the peritoneal cavity, compared with long asbestos fibers (Poland et al., 2008). Previously, we proposed that the characterization of the physical properties of nanomaterials in cell culture medium is essential for evaluating their influences on cellular processes (Horie & Fujita, 2011; Horie et al., 2012). By extension, we hypothesize that the physical properties of CNTs are critical for their pulmonary toxicity in exposed animals.

Among CNTs, single-wall carbon nanotubes (SWCNTs) have unique characteristics in terms of small diameter and thin flexible shapes. It is still unclear how the physical properties of SWCNTs are related to toxicity. After intratracheal SWCNT

instillation, *in vivo* experimental studies in rat lungs have been conducted to evaluate the acute pulmonary toxicity. Bronchoalveolar lavage fluid (BALF) analysis revealed that exposure to SWCNTs (5 mg/kg) produced transient inflammatory and cytotoxic effects for up to 1 month after instillation (Warheit et al., 2004). In an impurity-free SWCNT-exposed group of rats (2 mg/kg), acute lung inflammation and subsequent pulmonary granulomas accompanied by increased lung weights were observed, but no evidence of fibrosis, atypical lesions, or tumor-related findings was observed until 6 months post-instillation (Kobayashi et al., 2011). In our previous study, histopathological examinations, BALF analyses, and enzyme-linked immunosorbent assays (ELISAs) demonstrated that persistent pulmonary inflammation occurred in rat lungs up to 6 months following SWCNT instillation (0.2 mg or 0.4 mg per rat) (Morimoto et al., 2012). In addition, we observed gene expression changes in rat lungs for long-term periods after intratracheal instillation of SWCNTs (Fujita et al., 2014a). However, these tests were performed using SWCNTs of the same size, and the size effects were not determined.

The cytotoxicity of SWCNTs has been addressed in *in vitro* cell-based assay systems; however, the cytotoxic effects of SWCNTs remain controversial. Indeed, some researchers have reported an absence of cytotoxicity or induction of the inflammatory mediator interleukin 8 upon incubating a human alveolar epithelial cell line (A549) with SWCNTs (Pulskamp et al., 2007; Worle-Knirsch et al., 2006). Cytotoxicity assessments revealed that SWCNTs have very low toxicity in A549 cells (Davoren et al., 2007). In contrast, SWCNTs can inhibit the cell proliferation of A549, HaCaT human keratinocyte, HeLa human cervical cancer, and H1299 human lung carcinoma cells (Manna et al., 2005). Previously, we examined the effects of impurity-free SWCNTs with different physical properties on cellular responses in human alveolar epithelial A549 cells (Fujita et al., 2013). The results suggested that SWCNTs do not cause serious cytotoxicity; however, the physical properties, especially the size and the length of the bundles of SWCNTs dispersed in cell culture medium, contributed to a change in intracellular reactive oxygen species (ROS) generation.

We consider that intratracheal instillation studies are valuable for examining acute-phase inflammatory responses and recovery after SWCNT instillation (Fujita et al., 2014a). Specific length-dependent increases in the release of superoxide anions and pro-inflammatory cytokines occur in human monocytes treated with long-fiber-containing CNT samples (Brown et al., 2007). These findings suggest that phagocytic cells such as alveolar macrophages, which are responsible for the phagocytosis of foreign substances, are more sensitive to CNTs than epithelial cells. In this study, we examined the effects of the physical properties of SWCNTs on toxicity following *in vivo* rat intratracheal instillation tests and in *in vitro* cell-based assays using rat alveolar macrophage NR8383 cells. The SWCNTs were dispersed to provide working solutions with different physical properties, mainly in terms of diameter and length, and the physical properties contributing to toxicity were characterized both *in vivo* and *in vitro*.

The objective of this study was to determine the effect of size on the *in vivo* and *in vitro* toxicity of SWCNTs. One of the methodological issues that need to be resolved regarding SWCNT toxicity is the optimal method for dispersing SWCNTs with different sizes into working solutions for both *in vivo* and *in vitro* tests, in addition to the maintenance of their dispersion status. Some studies have reported that polymeric surfactants can be used for effectively dispersing CNTs in *in vivo* tests (Herzog et al., 2009; Mutlu et al., 2010; Wang et al., 2010). However, careful attention needs to be paid when using polymeric surfactants in terms of their potential cytotoxicity. Results in our recent study showed that the non-ionic surfactants Pluronic F127, 1,2-dipalmitoyl-sn-glycero-3-phosphocholine (DPPC), Surfacten, and Tween 80 caused an increase in intracellular ROS levels in A549 cells (Horie et al., 2013). To address this methodological problem, we sought to disperse SWCNTs with different sizes homogeneously in bovine serum albumin (BSA) without adding any synthetic surfactants based on our previous study (Fujita et al., 2013) and to characterize the physical properties of SWCNTs in working solutions for use in *in vivo* and *in vitro* tests. BSA solution is a suitable vehicle for most insoluble carbon nanotubes that need to be tested both *in vitro* and *in vivo* for their toxicological properties (Elgrabli et al., 2007).

Metallic impurities of CNTs inevitably remain during the synthesis process. Trace metals associated with commercial nanotubes are responsible for the biological effects (Pulskamp et al., 2007). A meta-analysis of nanotoxicity studies showed that CNT pulmonary toxicity is significantly increased but not dominated by the amounts of metallic impurities (Gernand & Casman, 2014). Thus, the effects of residual metallic impurities on pulmonary toxicity are still undetermined. In this study, we used impurity-free SWCNTs with high purity synthesized by water-assisted chemical vapor deposition (CVD). The high-efficiency synthetic process developed by adding a small and controlled amount of water during ambient SWCNT formation resulted in a massive growth of vertically aligned SWCNTs (a CNT ''forest'') from the catalyst surface (Hata et al., 2004). We consider that this synthesis procedure using impurity-free SWCNTs is advantageous for excluding the effects of catalytic residual metallic impurities on toxicity.

Materials and methods

Test materials and their preparation

SWCNTs were obtained from the Technology Research Association for Single-Wall Carbon Nanotubes (Japan). A Brunauer–Emmett–Teller (BET)-specific surface area of $1064 \pm 37\ m^2/g$ was measured as described previously (Kobayashi et al., 2011). The elemental carbon composition of SWCNTs was determined to be >99.0% (wt) by using a thermal gravimetric analyzer (TGA-50; Shimadzu, Kyoto, Japan). The Fe content (0.011% wt) was measured using an inductively coupled plasma mass spectrometry (ICP-MS) (ELEMENT XR™; Thermo Fisher Scientific Inc., Waltham, MA). A *G*/*D* ratio of 5.9 was determined using a Raman spectrometer (Thermo Fisher Scientific Inc., Waltham, MA). SWCNTs were dispersed in stock suspensions at an estimated concentration of 1.0 mg/mL in order to change their size, following two distinct protocols. The preparation was based on the protocols outlined in previous study (Fujita et al., 2013). In the first protocol, SWCNTs were dispersed into 10 mg/mL

BSA solution for 2 h, by using an ultrasonic homogenizer. SWCNTs were centrifuged, and the resulting supernatant was filtered through a cell strainer with a 40-μm nylon mesh (Becton, Dickinson & Company, Franklin Lakes, NJ). The filtrates were used as stock suspensions and designated ''CNT-1S.'' In the second protocol, SWCNTs were dispersed into a 10-mg/mL BSA solution for 30 min using an ultrasonic homogenizer. SWCNTs were centrifuged, and the supernatant was filtered through a cell strainer with a 70-μm nylon mesh and centrifuged again. The precipitates were re-dispersed into BSA solution within an operating ultrasonic bath. The mixtures were filtered using a cell strainer with a 100-μm nylon mesh (Becton, Dickinson & Company, Franklin Lakes, NJ). The filtrates were used as stock suspensions and designated ''CNT-2S.''

Characterization of SWCNTs

SWCNT working solutions (CNT-1 or CNT-2) were prepared by diluting stock suspensions (CNT-1S or CNT-2S) in phosphate-buffered saline (PBS) to 0.1 mg/mL (low dose: CNT-1(L) or CNT-2(L)) or 1.0 mg/mL (high dose: CNT-1(H) or CNT-2(H)) for use in *in vivo* rat intratracheal instillation tests. Stock suspensions were diluted to 0.1 mg/mL in cell culture medium for use in *in vitro* cell-based tests. The concentration of SWCNTs in stock suspensions or working solutions was determined by measuring their UV–Vis absorption spectra with a JASCO V7200DS spectrometer (JASCO Corporation, Tokyo, Japan) at wavelengths of 600–900 nm (Fujita et al., 2014b). The particle size of SWCNTs in working solutions was measured by dynamic light scattering (DLS) (Kato et al., 2009). The average particle diameter was determined using an FPAR-1000 Fiber-Optics Particle Analyzer (Otsuka Electronics Co., Osaka, Japan). Samples were maintained at 1 cm from the surface of the solutions in static 15-mL tubes. The viscosity of the dispersions was determined using an Ubbelohde Viscometer, Size 0 (Sibata Scientific Technology, Tokyo, Japan). The observed values were used for DLS and zeta-potential assessments. The zeta potential of the SWCNTs dispersed in working solutions was measured using an ELS-Z Zeta-potential & Particle Size Analyzer (Otsuka Electronics Co., Osaka, Japan). The *G*/*D* ratio was determined using a DXR Raman Microscope recorded with a 532-nm laser line (Thermo Fisher Scientific Inc., Waltham, MA). The length of SWCNTs in stock suspensions or working solutions was measured by TEM-based observations of 1000 SWCNT bundles.

In vivo rat intratracheal instillation test

Animals and experimental design

Nine-week-old male Wistar rats purchased from Japan SLC, Inc. (Shizuoka, Japan) were stratified into three groups ($n = 9$ per group per time point). The average rat body weight before the instillation treatment was approximately 220 g. Groups of rats were anesthetized and intratracheally administered to a low-dose SWCNT working solutions (CNT-1(L) or CNT-2(L): approximately 0.18 mg/kg) or high-dose SWCNT working solutions (CNT-1(H) or CNT-2(H): approximately 1.8 mg/kg). The vehicle control group was administered 0.4 mL of 10 mg/mL BSA solution/rat. After intratracheal instillation treatment, rats were housed within polycarbonate cages at a controlled temperature of 23 °C and fed a chow diet *ad libitum*. After the instillation, the viabilities and general conditions of rats were observed once a day until they were sacrificed. The body weight of each rat was measured before instillation and at 1, 3, 7, 30, and 90 d post-exposure. Morphological observation, BALF analysis, histopathological analysis, and comprehensive gene expression microarray analysis were performed on dissected lungs at 1, 3, 7, 30, and 90 d post-instillation. All procedures and animal handling were performed by the Public Interest Incorporated Foundation at the Biosafety Research Center in Shizuoka, Japan, according to the guidelines described in the Japanese Guide for the Care and Use of Laboratory Animals as approved by the Animal Care and Use Committee.

Cytokine assays and cell counts with BALFs

Rats were anesthetized by isoflurane (Mylan Inc., Tokyo, Japan) and euthanized by exsanguination. The left bronchus was clamped with forceps and the right bronchus was cannulated. Subsequently, 3 mL of heated (37 °C) saline (Otsuka Pharmaceutical Factory, Inc., Tokushima, Japan) was filled and aspirated to and from the lung to recover BALF fractions. This procedure was repeated three times. Supernatants were obtained by centrifuging BALFs at $250 \times g$ for 10 min and were used for total protein and cytokine measurements. Total protein concentrations in BALF supernatants were measured with an automatic biochemical analyzer (7170; Hitachi High-Tech Fielding Corporation, Tokyo, Japan). Since the cytokine macrophage inflammatory protein-1α (MIP-1α) is a major factor produced by alveolar macrophages during early stages of the inflammatory response, the levels were measured using a MILLIPLEX® MAP Rat Cytokine/Chemokine Magnetic Bead Panel and Luminex 200 System (Merck Millipore, Billerica, MA). The cell fraction suspended in PBS was used to determine cell counts in BALF samples. The total number of cells in BALF was counted using a hematology system (ADVIA120; Siemens Healthcare diagnostics, Inc., Tokyo, Japan). The number of neutrophils, lymphocytes, eosinophils, and macrophages were counted on the May-Grünwald-Giemsa staining. At microscopic examination, phagocytosing macrophages and non-phagocytosing macrophages were identified as atypical and normal macrophages, respectively.

Histopathological analysis

After rats were sacrificed, their left lungs were processed for histopathological studies. Lung tissues were fixed in 4% buffered paraformaldehyde, embedded in paraffin, and stained with hematoxylin and eosin. Digital images of each lung section focused on the alveoli, alveolar walls, bronchioles, and vessels for histopathological evaluation.

Cell-based *in vitro* assay

Cell culture and exposure to CNTs

Stock suspensions (1.0 mg/mL) of CNT-1S and CNT-2S were diluted 10-fold in Ham's F-12K (Kaighn's) culture medium

(Life Technologies Japan Ltd., Tokyo, Japan), supplemented with 15% (v/v) heat-inactivated fetal bovine serum (FBS; Hana-Nesco Bio, Tokyo, Japan), 100 units/mL penicillin, and 100 units/mL streptomycin (from this point onwards this medium is referred to as F-12K + FBS medium). These working solutions were designated as CNT-1 and CNT-2 for *in vitro* cell-based assays. NR8383 rat alveolar macrophage cells obtained from American Type Culture Collection (CRL-2192; ATCC, Manassas, VA) were cultured at 37 °C in 25-cm^2 cell culture flasks in F-12K + FBS medium in a humidified atmosphere containing 5% CO_2. NR8383 cells were seeded into separate wells of 96-well plates (Becton, Dickinson & Company, Franklin Lakes, NJ) and grown in F-12K + FBS medium for 24 h. After centrifugation, the F-12K + FBS medium was removed and replaced by the working solutions (CNT-1 or CNT-2). The cell density at the time of replacement of the working solutions was approximately 2×10^5 cells/mL.

Assessment of cell viabilities

An assay based on the use of 2-(4-iodophenyl)-3-(4-nitrophenyl)-5-(2,4-disulfophenyl)-2H-tetrazolium, monosodium salt (WST-1; Takara Bio Inc., Otsu, Japan) to detect mitochondrial dehydrogenase activity was used as an indicator of cell viability. After treatment of cells with CNT-1 and CNT-2 in quadruplicate, the supernatant was removed. WST-1, diluted 1:10 (v/v) with F-12K + FBS medium, was then added to each well of 96-well plates, and samples were incubated for 1 h at 37 °C. Sample absorbance at 450 nm was measured in a Model 680 microplate reader (Bio-Rad Laboratories, Tokyo, Japan), using the absorbance at 750 nm as a reference. Data were normalized to absorbance values for untreated control cells treated with F-12 + FBS medium containing 1.0 mg/mL BSA.

Measurement of intracellular ROS

Intracellular ROS were detected by 2′,7′-dichlorofluorescein diacetate (DCFH-DA) assay using the OxiSelect™ Intracellular ROS Assay Kit (Cell Biolabs, Inc., San Diego, CA). After treatment, DCFH-DA dissolved in culture medium was added to NR8383 cells and the cells were incubated for 6 h at 37 °C. The cells were then washed with PBS and resuspended in cell lysis buffer. The fluorescence was measured, with excitation and emission wavelengths of 480 nm and 530 nm, respectively, using a Gemini™ XPS microplate reader (Molecular Devices, LLC, Silicon Valley, CA).

Cytokine assays

MIP-1α expression levels were measured using a MILLIPLEX® MAP Rat Cytokine/Chemokine Magnetic Bead Panel and Luminex 200 System (Merck Millipore, Billerica, MA).

TEM observations

In *in vivo* rat intratracheal instillation tests, mediastinal lymph nodes were fixed using 2.5% (v/v) glutaraldehyde for 2 h at 4 °C and 1% osmium oxide solution for 2 h at 4 °C, dehydrated in ethanol, and embedded in a commercially available epoxy resin (TAAB Laboratories Equipment Ltd., Reading, England). Samples were transferred to fresh resin in capsules and polymerized at 60 °C for 48 h. In *in vitro* cell-based assays, after treatment, cells were fixed sequentially in 1.2% (v/v) glutaraldehyde for 1 h at 20 °C and in 1% osmium oxide solution for 1 h at 4 °C, dehydrated in ethanol, and embedded in a commercially available epoxy resin (TAAB Laboratories Equipment Ltd., Reading, England). Samples were transferred to fresh resin in capsules and polymerized at 60 °C for over 48 h. A transmission electron microscopy (TEM) system at 75 kV (H-7000; Hitachi, Tokyo, Japan) was used to observe the intracellular distribution of SWCNTs and morphologic changes in the mediastinal lymph nodes of rats and in NR8383 cells.

RNA extraction and DNA microarray experiments

Right lungs ($n = 4$ per group per time point) were homogenized using the QIAzol Lysis Reagent and a TissueRuptor (Qiagen, Tokyo, Japan). Total RNA from homogenates was extracted using the RNeasy Midi Kit (Qiagen, Tokyo, Japan), following the instructions of the manufacturer. Cells incubated in the presence or absence of CNT-1 or CNT-2 ($n = 4$) were collected, and the total RNA was extracted from the cells using the RNeasy Mini Kit (Qiagen, Tokyo, Japan), following the instructions of the manufacturer. RNA was quantified using a NanoDrop 2000 spectrophotometer (Thermo Fisher Scientific Inc., Waltham, MA), and sample qualities were monitored with the Agilent 2100 Bioanalyzer (Agilent Technologies, Santa Clara, CA). Cyanine-3-labeled cRNA was prepared from RNA using the One-Color Low RNA Input Linear Amplification PLUS Kit (Agilent Technologies, Santa Clara, CA), according to the instructions of the manufacturer, followed by RNeasy column purification (Qiagen, Tokyo, Japan). Each labeled cRNA probe was used separately for hybridization to a 4×44 K Whole Rat Genome Microarray Kit (G4131F; Agilent Technologies, Santa Clara, CA), and hybridization was performed at 65 °C for 17 h. Hybridized microarray slides were washed according to the instructions of the manufacturer and were scanned with an Agilent DNA Microarray Scanner (G2565BA; Agilent Technologies, Santa Clara, CA) at 5-μm resolution. The scanned images were analyzed numerically using Agilent Feature Extraction Software, version 10.7.3.1 (Agilent Technologies, Santa Clara, CA).

Microarray data analysis

Normalized data were analyzed using GeneSpring GX software, version 11.5.1 (Agilent Technologies, Santa Clara, CA). Log fold-changes represent the ratio of the normalized intensity values of CNT-1 or CNT-2-exposed samples to the normalized intensity value of vehicle control samples. Genes displaying log fold-change values ≥ 1 were considered as upregulated genes, whereas those displaying values ≤ -1 were considered downregulated genes. Gene expression data for each experimental group were deposited into the Gene Expression Omnibus database (Accession number GSE61483 and GSE61319; http://www.ncbi.nlm.nih.gov/projects/geo/). The web-based application GOstat (http://gostat.wehi.edu.au/)

was used to identify statistically overrepresented Gene Ontology (GO) terms (Beissbarth & Speed, 2004) with the Rat Genome Database (RGD: http://rgd.mcw.edu/). Differences between control and experimental groups were evaluated using the unequal variance Welch *t* test, which is suitable regardless of whether two groups have a similar or dissimilar variance. *p* Values ≤ 0.05 were considered statistically significant.

Statistical analysis

All numerical values are represented as mean ± SD. Statistical significances of the differences between the data obtained using treated samples and untreated controls were determined by analysis of variance (ANOVA), using the Dunnett or the Steel test for multiple comparisons. Significance was set at $p \leq 0.01$ or $p \leq 0.05$.

Results

Characterization of SWCNTs dispersed in working solutions

We prepared two types of dispersions of SWCNTs with different sizes to elucidate the effect of size on *in vivo* and *in vitro* toxicities. The characterization of SWCNTs in working solutions for *in vivo* and *in vitro* tests is shown in Figure 1. Analysis with an absorption spectrometer demonstrated nearly equivalent SWCNT concentrations in the adjusted working solutions (approximately 0.1 mg/mL and 1.0 mg/mL for *in vivo* tests; approximately 0.1 mg/mL for *in vitro* cell-based assays). DLS and zeta-potential studies revealed the average diameters of the dispersed SWCNT particles and the dispersibility/aggregability characteristics of CNT-1 and CNT-2. These analyses confirmed that SWCNT particles were stable and dispersed in the working solutions. DLS results confirmed that no significant changes occurred in the light scattering intensity-averaged diameter of SWCNTs in cell culture medium for 3 d after preparation (data not shown); thus, working solutions were used within 3 d after preparation for *in vitro* cell-based assays. Furthermore, no significant difference was found in the average diameter of SWCNTs in both stock suspensions stored at 4 °C for 8 weeks after preparation (data not shown). Working solutions were used within 7 d after preparation for *in vivo* tests. The negative zeta potential of all adjusted samples revealed that SWCNT particles were well dispersed in working solutions. Raman spectrophotometric analysis revealed that the *G*/*D* ratio for bulk SWCNTs was reduced slightly, from 5.9 to 4.1 or 2.4 for CNT-1 or CNT-2, respectively. ICP-MS results revealed that the metal content (e.g. Fe, Y, and Ni) of CNT-1 and CNT-2 was at an undetectable level. Previously, we demonstrated that the adsorption of proteins by ultrafine metal oxide particles influences their cytotoxicity to cultured cells (Horie et al., 2009). There was no significant reduction of salt concentrations (e.g. Na, P, and Ca) in CNT-1 and CNT-2 in culture medium (data not shown). TEM images of representative SWCNT dispersions showed differences in their lengths in working solutions, designated here as CNT-1 and CNT-2. CNT-1 was observed to contain relatively thick SWCNT structures with a short linear shape (Figure 1A, B, and F). The nanotubes in the CNT-2 working solution assembled into relatively thick bundles of SWCNTs with a long linear shape (Figure 1D, E, and G). Noticeably aggregated forms of SWCNTs in each working solution were not identified. These studies revealed that CNT-1 and CNT-2 were stably dispersed and assembled into relatively thick bundles with a long linear shape (CNT-1) or into relatively thin bundles with a short linear shape (CNT-2) in working solutions. The preparation procedure described in this study may thus be valuable for use in both *in vivo* and *in vivo* studies.

BALF analysis

Lungs of anesthetized rats were excised and subjected to BALF analysis at 1, 3, 7, 30, and 90 d post-instillation. Total protein levels in the group exposed to a high dose of CNT-1 were significantly increased at 1 d post-instillation ($p < 0.05$) and further increased over time. In contrast, the high levels of total protein observed at 1 d post-instillation ($p < 0.01$) decreased over time in the group exposed to a high dose of CNT-2 (Figure 2A). MIP-1α levels were elevated during the observation period in groups exposed to a high dose of CNT-1 or CNT-2 (Figure 2B). Notably, significantly high MIP-1α levels in the group exposed to a high dose of CNT-1 were observed at 30 and 90 d post-instillation ($p < 0.01$).

Normal macrophages were dominant in the total nucleated cells from the vehicle control group during the observation period (Figure 3A, C, and E). Total nucleated cells and neutrophil counts in BALF from the low- and high-dose CNT-1-exposed group and those from the high-dose CNT-2-exposed group increased during the observation period (Figure 3A and B). These results show that neutrophils in the group exposed to a high dose of CNT-1 were dominant among the total nucleated cells during the observation period (Figure 3E). The amount of lymphocytes in the high-dose CNT-1 or CNT-2 groups was significantly increased at 7 d post-instillation ($p < 0.05$ or $p < 0.01$, respectively; data not shown). Slightly increased eosinophil counts in BALF from the high-dose CNT-2 group were also observed (data not shown). The amount of normal macrophages in BALF from the CNT-1 and CNT-2 groups was significantly higher compared with levels observed in the vehicle control group at 30 d post-instillation ($p < 0.01$) (Figure 3C). The high-dose CNT-1 group showed an increase in the number of atypical macrophages at days 30 and 90 post-instillation (Figure 3D). In contrast, the number of normal and atypical macrophages of the high-dose CNT-2 group increased until 30 d post-instillation (Figure 3C and D). The results show that normal and atypical macrophages in the group exposed to a high dose of CNT-2 were dominant among the total nucleated cells after at 3 d post-instillation (Figure 3E). Total protein levels, MIP-1α expression, and cell counts in BALF examinations revealed that CNT-1 caused pulmonary inflammation and slower recovery and that CNT-2 elicited acute lung inflammation shortly after their instillation.

Anatomical observations after instillation with SWCNTs

Autopsy confirmed that SWCNT aggregates (black, brown, gray, red, or white patches) were present in dissected lungs

(A)

Sample			Concentration of SWCNTs (mg/mL)	Particle size (nm)		Zeta potential (mV)	G/D ratio	Length* (μm)
				d_l	d_n			
CNT-1	*in vivo* test	Low dose	0.11	352.2	141.9	-27.6	NT	NT
		High dose	1.03	404.4	167.2	NT	2.4	0.51 (0.36)
	in vitro test		0.10	380.8	132.8	-13.7	4.1	0.36 (0.31)
CNT-2	*in vivo* test	Low dose	0.11	1151.3	413.6	-29.9	NT	NT
		High dose	1.10	1534.2	584.5	NT	2.6	1.67 (1.53)
	in vitro test		0.11	1069.7	407.5	-12.0	3.9	1.52 (1.99)

d_l: Light scattering intensity-averaged diameter; d_n: Number-averaged diameter. *Values are expressed as arithmetic mean (arithmetic standard deviation). The length for *in vitro* tests was measured in the stock solution. NT: not tested.

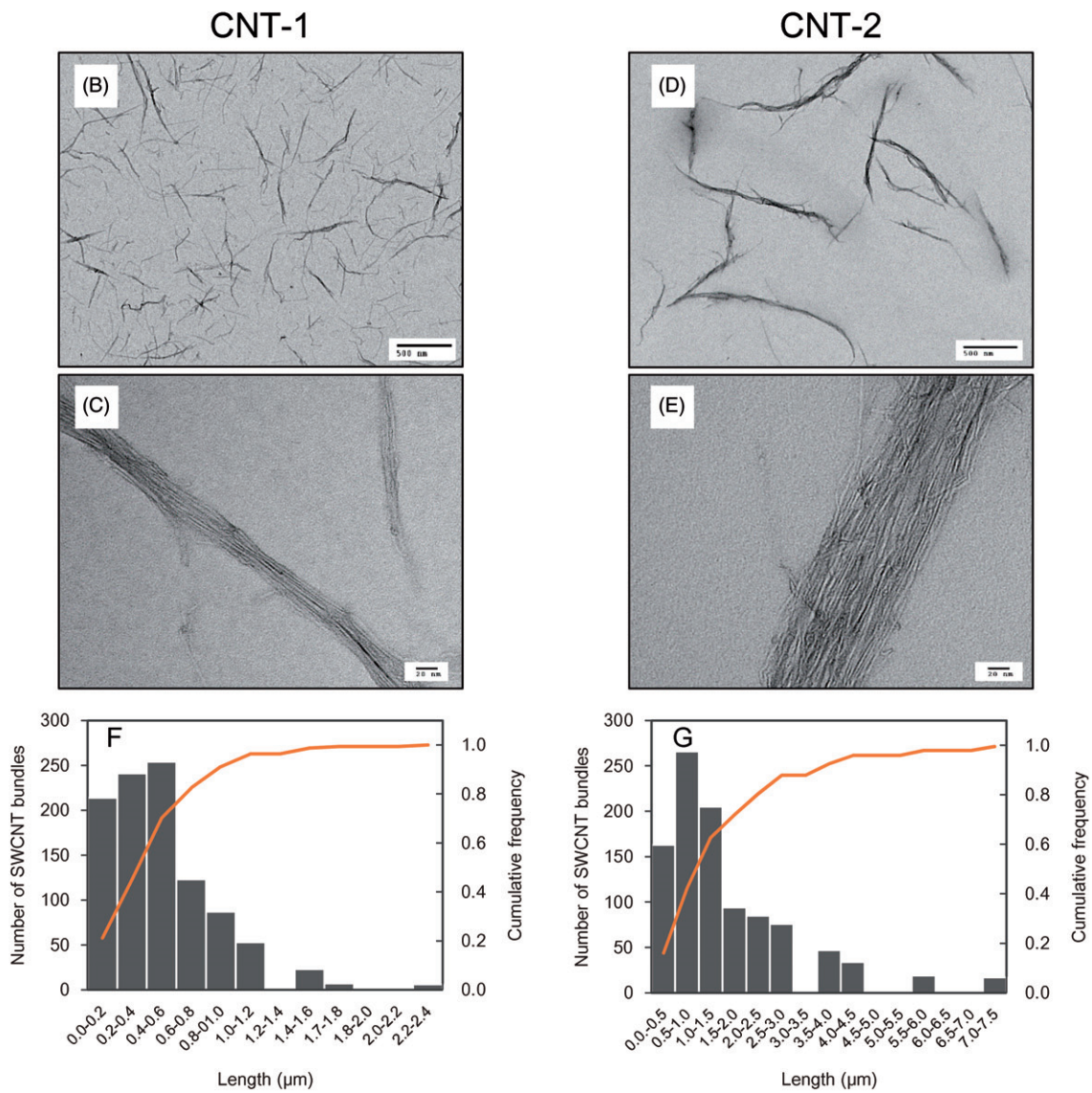

Figure 1. Characterization of SWCNTs dispersed in working solutions. Characterization of SWCNTs in working solutions for *in vivo* and *in vitro* tests (A). TEM images of SWCNTs in CNT-1 (B and C) and CNT-2 (D and E) in working solutions for *in vivo* (high dose) studies. High-magnification micrographs (C and E). Distribution of SWCNT length in working solutions for *in vivo* (high dose) evaluation by digital TEM images (F and G).

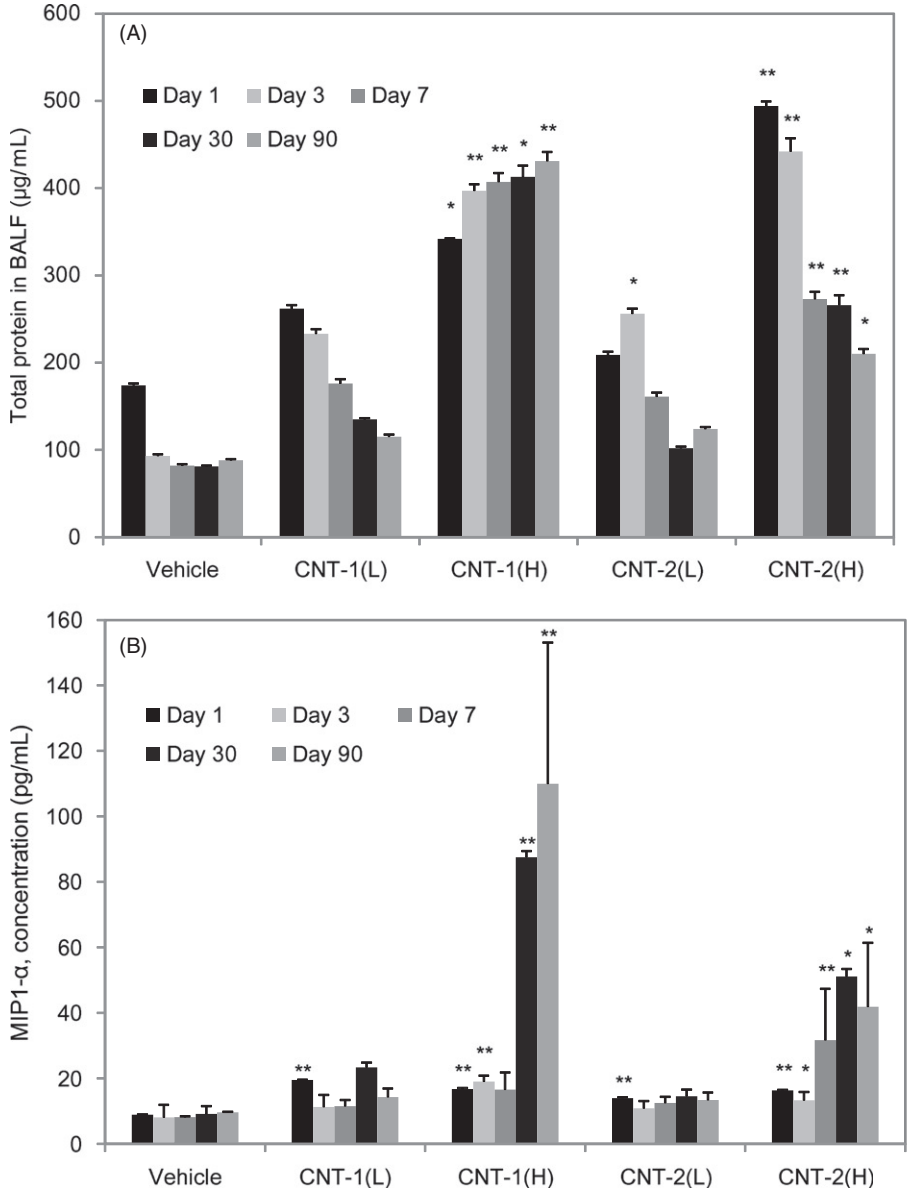

Figure 2. Total protein content and MIP-1α in BALFs following exposure of rats to CNT-1, CNT-2, or vehicle controls at the indicated time points. Total protein content (A) and the levels of MIP-1α (B) in the BALF following exposure of rats to CNT-1, CNT-2, or vehicle controls at each time point. Values are represented as the mean ± SD. The asterisk indicates a statistically significant difference compared to the vehicle control group (multiple permutation-based Welch test, $*p < 0.05$, $**p < 0.01$).

from the CNT-1 or CNT-2 groups during the observation period, whereas no obvious morphological changes were observed in the vehicle control group. SWCNT aggregates were not completely eliminated at 90 d post-instillation (Figure 4A).

Histopathological findings in lungs stained with hematoxylin and eosin in the high-dose CNT-1 and CNT-2 groups and their severity scores at 1, 3, 7, 30, and 90 d post-instillation are discussed below. Average lesion severity scores assigned to individual animals were determined from a complete pathological examination and were recorded (0, not remarkable; 1, slight; 2, moderate; and 3, marked; based upon relative evaluation of lesions). At 1, 3, and 7 d post-instillation, the scores for focal inflammatory changes (alveolitis) and macrophage increases in the high-dose CNT-2 group were higher than those in the high-dose CNT-1 group at 3 d post-instillation. The scores for infiltration of neutrophils into alveoli in the CNT-1 group were higher than those in the CNT-2 group at 7 d post-instillation (Table 1). The CNT-1 and CNT-2 test substances were interspersed in alveoli, and persistence of SWCNT aggregate-laden macrophages was observed in the alveoli at 1 d post-instillation in both groups (Figure 4B1 and B2) and at 3 d post-instillation in the CNT-1 group (Figure 4B3). Infiltrating eosinophils were observed in the perivascular and peribronchial interstitial spaces (data not shown). The amount of foamy macrophages in pulmonary alveoli and intra-alveolar hemorrhages increased over time (Figure 4B5). Macrophage-containing granulomas around the sites of CNT-2 aggregates had accumulated by 3 d post-instillation (Figure 4B4). This phenomenon continued up to 90 d (Figure 4B6, B8, and B10). Foamy macrophage and granuloma scores in the CNT-2 group were obtained at 3 or 7 d post-instillation, whereas those in the CNT-1 group were obtained at 30 d post-instillation (Table 1). Gross pathology of the lung nodules, abnormal white patches, and whitening of the lung tissues were observed. In addition, black, gray, red, browning, patched, and enlarged lymph nodes were occasionally observed. The extent of these findings was dependent on the dose of CNT-1 or CNT-2 administered (data not shown). At 30 d post-instillation, infiltrating eosinophils were no longer observed in the perivascular and peribronchial interstitial spaces. Cell debris, presumably from disruptions

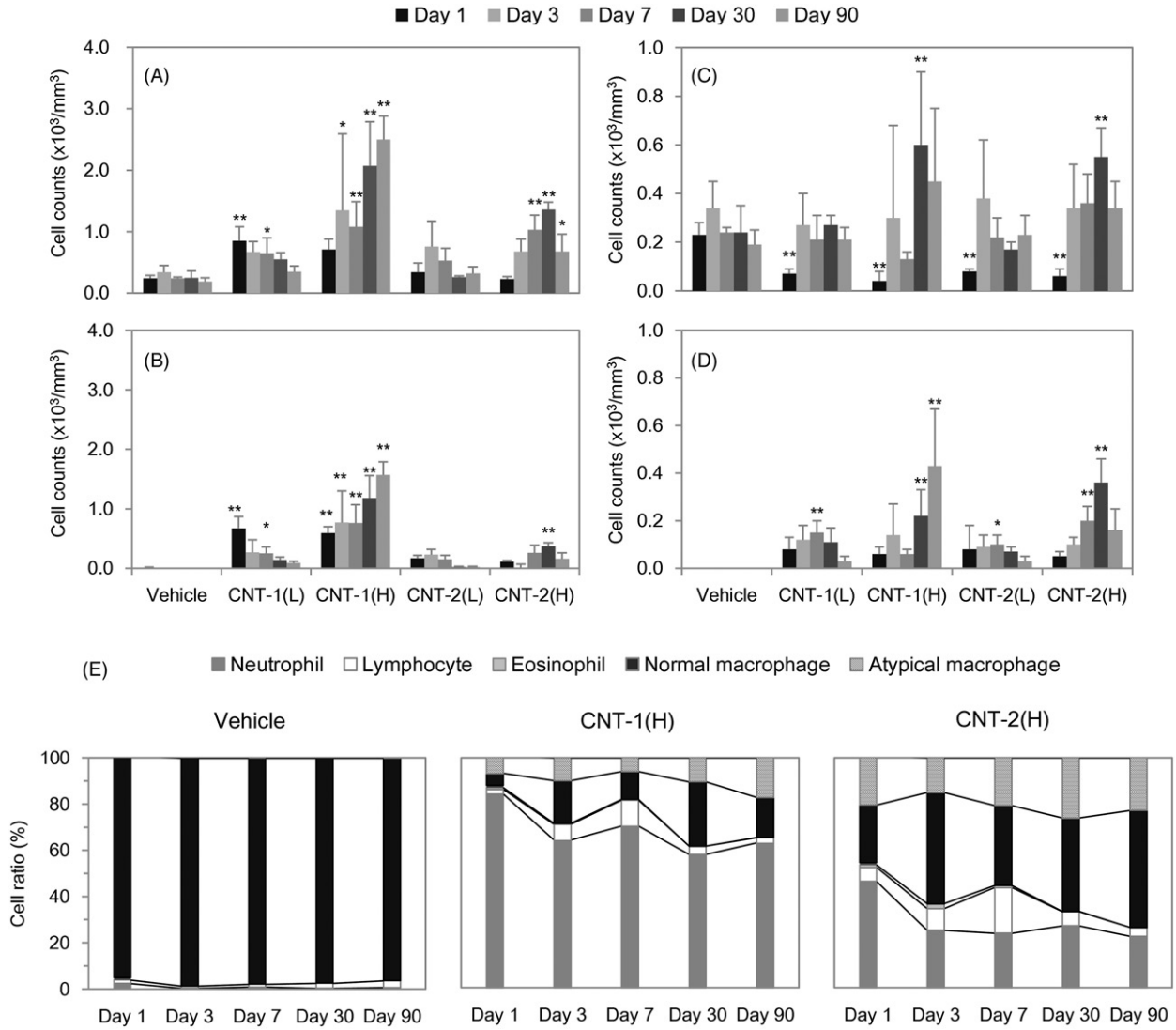

Figure 3. Cell counts in BALF following exposure of rats to CNT-1, CNT-2, or vehicle controls at each time point. Total nucleated cell (A), neutrophil (B), normal macrophage (C), and atypical macrophage (D) counts in BALF following exposure of rats to CNT-1, CNT-2, or vehicle controls at each time point. Values are represented as the mean ± SD ($\times 10^3$/mm^3). Asterisk indicates a statistically significant difference compared to the vehicle control group (multiple permutation-based Welch test, $*p<0.05$, $**p<0.01$). Percentage of neutrophils, lymphocytes, eosinophils, normal macrophages, and atypical macrophages in BALF (E).

caused by macrophages infiltrating the alveoli, was observed in the low- and high-dose CNT-1 groups and in the high-dose CNT-2 group. Cell debris scores in the alveoli of rats exposed to CNT-1 were high at 30 and 90 d post-instillation. Focal inflammatory changes, neutrophil infiltration into alveoli, increased macrophage proportion, persistence of SWCNT aggregate-laden macrophages, and foamy macrophages were observed in the CNT-1 and CNT-2 groups (Table 1). Macrophage-containing granulomas around the sites of CNT-1 aggregates had accumulated by 30 d post-instillation (Figure 4B7). At 90 d post-instillation, focal inflammatory changes, persistence of macrophages laden with SWCNT aggregates as granular substances, and foamy macrophages were observed in both SWCNT groups (Figure 4B9 and 4B10). The scores for focal inflammatory changes, infiltration of neutrophils into alveoli, macrophage increases, macrophage test substance engulfment, foamy macrophages, and cell debris in alveoli in the CNT-1 group were higher than those in the CNT-2 group at 90 d post-instillation (Table 1).

TEM analysis showed that SWCNT bundles were present in mediastinal lymph nodes in the high-dose CNT-1 and CNT-2 groups at 90 d post-instillation (Figure 5). Some SWCNT bundles similar to those shown in Figure 1 were observed. No fiber tangle formation was identified.

Gene expression profiling results from *in vivo* rat intratracheal instillation tests

Comprehensive analysis of gene expression profiles using a DNA microarray revealed time-dependent changes in gene expression in rat lungs intratracheally instilled with a high dose of CNT-1 or CNT-2. DNA microarray data from these experiments were deposited in the Gene Expression Omnibus database, under accession no. GSE61483. The number of genes that were significantly upregulated ($FC>1$) or downregulated ($FC<-1$) with $p \leq 0.05$ at each time point was determined, as shown in Figure 6(A). The number of genes in

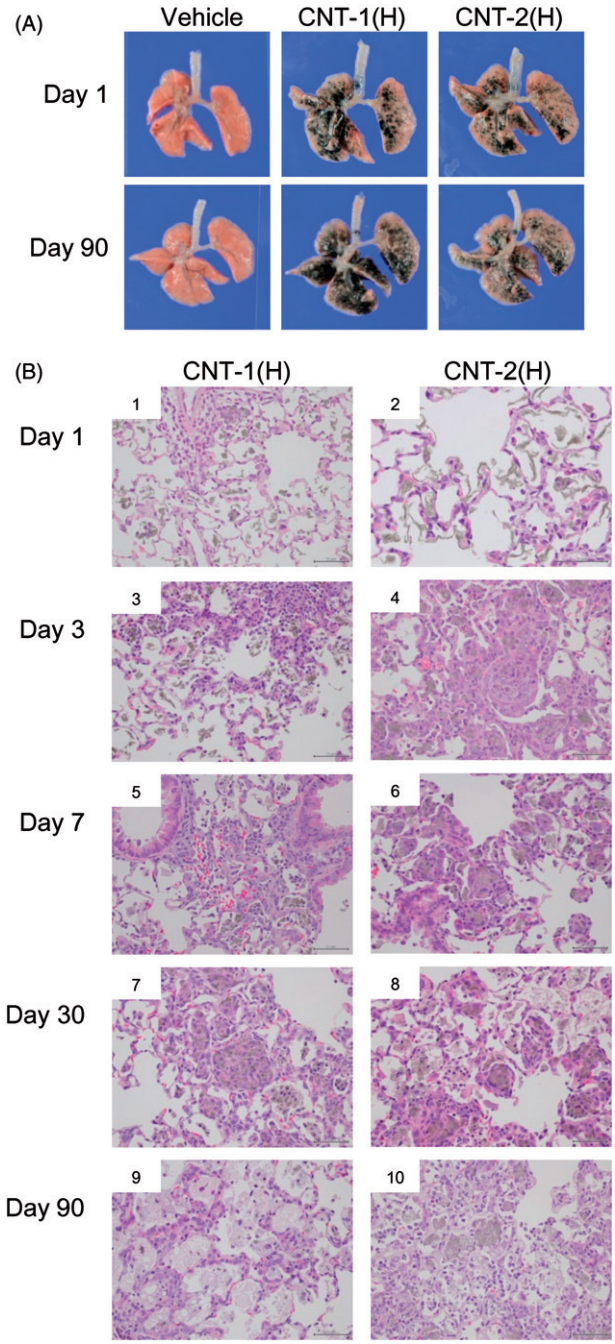

Figure 4. Anatomical observations after instillation with SWCNTs. Dissected lungs from a rat exposed to SWCNTs at 1 and 90 d post-instillation (A). The lungs were dissected at each time point post-instillation from groups of rats exposed to the vehicle control or a high dose of CNT-1 or CNT-2. Micrographs of lung tissue from rats exposed to CNT-1 or CNT-2 at a high dose at 1, 3, 7, 30, and 90 d post-instillation (B).

the high-dose CNT-1 group was relatively constant throughout the observation period. However, many upregulated and downregulated genes were observed in the CNT-2 group at 1 d post-instillation, and this differential regulation was decreased by 3 d post-instillation. The number of differentially expressed genes in the CNT-2 group was similar to that in the CNT-1 group at 7 d post-instillation. The number of upregulated and downregulated genes in the CNT-1 group was higher than that in the CNT-2 group at 30 and 90 d post-instillation.

Next, we determined time-dependent changes in p values of the statistically overrepresented GO terms ''inflammatory response'' (GO: 0006954), ''cell proliferation'' (GO: 0008283), and ''immune system process'' (GO: 0002376; Figure 6B). The minus log p values of these GO terms for CNT-2-induced genes were higher than those for the CNT-1-induced genes at 1 d post-instillation. However, the inflammatory response category was associated with extremely low –log p values at 30 d post-instillation with the CNT-1-induced genes. Similarly, the ''cell proliferation'' or ''immune system process'' GO terms were more overrepresented among CNT-1-induced genes than among CNT-2-induced genes at 7 or 30 d post-instillation, respectively. These results suggest that CNT-2-induced genes were intimately involved in inflammatory responses, cell proliferation, and immune system processes at 1 d post-instillation, whereas CNT-1-induced genes were strongly associated with these GO categories at 7 or 30 d post-instillation.

The results were confirmed by measuring the induction levels of individually upregulated genes involved in inflammatory responses at 1, 3, and 90 d post-instillation with CNT-1 or CNT-2 (Figure 6C). Genes encoding the complement proteins C3, C4bpa, and C4bpb exhibited high-level induction in the CNT-2 group at 1 d post-instillation. However, levels in the CNT-1 group were higher than those in CNT-2 group at 3 or 90 d post-instillation. In addition, several genes in the CNT-2 group were highly upregulated at 1 d post-instillation, including *Ccl2*, *Ccl3*, *Ccl4*, *Ccl7*, *Ccl9*, *Ccl12*, *Ccl17*, *Ccl22*, the chemokine (C-X-C motif) ligand gene *Cxcl2*, and *Cxcl3*. The degree of upregulation in the CNT-1 group at 3 or 90 d post-instillation was higher than that found with the CNT-2 group. Representative downregulated genes involved in inflammatory responses that displayed log-fold changes ≤ 1 were not observed (data not shown).

Effects of SWCNTs on cell viability, intracellular ROS levels, and MIP-1α expression

The effects of CNT-1 or CNT-2 on cell viability in NR8383 cells exposed to either working solution for 6 or 24 h were determined using a WST-1-based viability assay. The results indicated that CNT-1 or CNT-2 had little effect on cell viability after 6 h (Figure 7A). However, NR8383 cell viability was significantly decreased following a 24-h exposure to CNT-2. The levels of intracellular ROS were measured in cells exposed to CNT-1 or CNT-2 for 6 or 24 h using the DCFH-DA assay (Figure 7B). Significantly elevated expression levels of the pro-inflammatory cytokine MIP-1α were observed at 6 h post-treatment with CNT-1 or CNT-2, and the levels at 24 h in CNT-2-treated cells were significantly higher than those of the controls (Figure 7C).

Cellular morphology and phagocytic uptake of SWCNTs

NR8383 cells were exposed to CNT-1 or CNT-2 for 24 h and then the phagocytic uptake of SWCNTs was observed by TEM. CNT-1, relatively thin bundles of SWCNTs with a short linear shape (Figure 8A and B), and CNT-2, relatively

Table 1. Pulmonary histopathology severity scores of rats exposed to CNT-1 or CNT-2.

			CNT-1 exposed group		CNT-2 exposed group	
	Time point	Vehicle control group	CNT-1(L)	CNT-1(H)	CNT-2(L)	CNT-2(H)
Focal inflammatory change (alveolitis)	Day 1	0	1.0	1.0	1.0	1.0
	Day 3	0	1.0	1.2	1.6	2.2
	Day 7	0	1.5	2.2	1.3	2.0
	Day 30	0	1.0	2.2	0	2.4
	Day 90	0	1.0	2.4	1.0	1.4
Infiltration, neutrophilic, alveolus	Day 1	0	1.0	1.6	1.0	1.0
	Day 3	0	1.5	1.6	2.0	1.8
	Day 7	0	2.0	2.2	1.2	1.4
	Day 30	0	1.8	2.6	0	2.0
	Day 90	0	1.0	2.2	0	1.8
Infiltration, eosinophilic, perivascular	Day 1	0	1.0	2.4	1.5	2.2
	Day 3	0	1.3	2.0	1.6	1.6
	Day 7	0	2.0	2.0	1.3	2.0
	Day 30	0	0	0	0	0
	Day 90	0	0	0	0	0
Infiltration, eosinophilic, peribronchial	Day 1	0	1.0	1.4	1.0	1.6
	Day 3	0	1.3	1.2	1.3	1.2
	Day 7	0	1.3	1.6	1.3	1.8
	Day 30	0	0	0	0	0
	Day 90	0	0	0	0	0
Increase, macrophage	Day 1	0	1.0	1.0	0	1.0
	Day 3	0	1.0	1.4	1.6	2.2
	Day 7	0	2.2	2.2	1.2	2.4
	Day 30	0	2.0	2.8	1.0	2.6
	Day 90	0	1.2	2.6	1.0	2.2
Macrophage engulfing test substance	Day 1	0	1.0	1.0	1.0	1.2
	Day 3	0	1.0	1.0	1.0	2.0
	Day 7	0	1.8	1.8	1.0	1.8
	Day 30	0	1.0	1.8	1.0	2.0
	Day 90	0	1.0	2.4	1.0	2.2
Foamy macrophage	Day 1	0	0	0	0	0
	Day 3	0	1.0	0	1.0	0
	Day 7	0	0	0	1.0	1.0
	Day 30	0	1.8	2.8	0	1.6
	Day 90	0	1.0	3.0	1.0	2.0
Granuloma	Day 1	0	0	0	0	0
	Day 3	0	0	0	0	1.0
	Day 7	0	0	0	0	1.2
	Day 30	0	0	2.0	0	1.0
	Day 90	0	0	0	0	1.5
Cell debris, alveolus	Day 1	0	0	0	0	0
	Day 3	0	0	0	0	0
	Day 7	0	0	0	0	0
	Day 30	0	1.0	2.6	0	1.3
	Day 90	0	0	2.8	0	1.4
Hemorrhage, alveolus	Day 1	0	1.0	1.0	1.0	2.0
	Day 3	0	0	0	1.0	1.0
	Day 7	0	0	1.0	1.0	1.0
	Day 30	0	0	0	0	0
	Day 90	0	0	0	0	0

An average severity scores given to individual animals was calculated from a complete pathological examination are 0, not remarkable; 1, slight; 2, moderate; and 3, marked; based upon relative evaluation of lesions.

thick bundles of SWCNT with a long linear shape (Figure 8C and D), were observed in the phagosome of cells exposed to SWCNTs for 24 h. Similarly, the phagocytic uptake of SWCNTs was observed in the phagosome of cells exposed to CNT-1 or CNT-2 for 6 h (data not shown). These results suggested that SWCNTs were translocated to the phagosome, maintaining their physical structure. No SWCNTs were observed within the nucleus in any of the samples.

Gene expression profiling for *in vitro* cell-based assays

Comprehensive analysis of gene expression profiles using a DNA microarray revealed the fold-changes in gene expression in NR8383 cells exposed to CNT-1 or CNT-2. DNA microarray data were deposited in the Gene Expression Omnibus database under accession no. GSE61319. The numbers of genes that were significantly upregulated ($FC > 1$) or downregulated ($FC < -1$) with $p \leq 0.05$

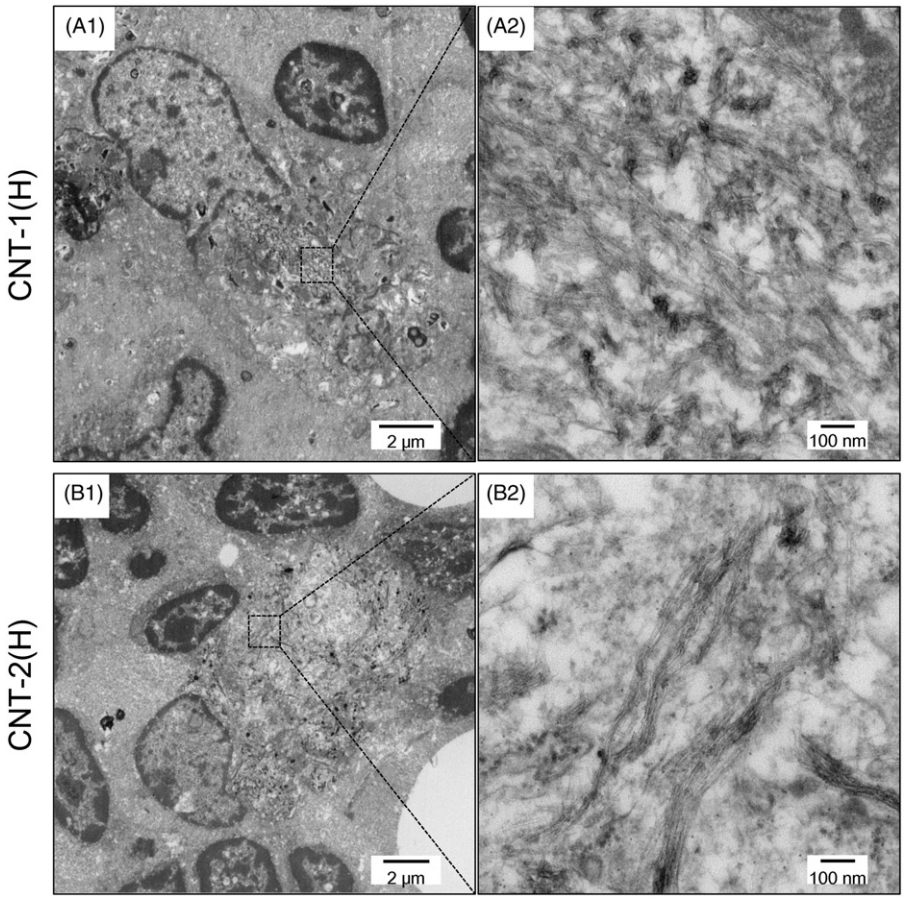

Figure 5. TEM images of mediastinal lymph nodes from rats exposed to CNT-1 or CNT-2 at a high dose at 90 d post-instillation. The mediastinal lymph nodes in the rats were fixed using 2.5% (v/v) glutaraldehyde for 2 h at 4 °C and 1% osmium oxide solution for 2 h at 4 °C, dehydrated in ethanol, and embedded in a commercially available epoxy resin. Samples were transferred to fresh resin in capsules and polymerized at 60 °C for 48 h. The TEM system was used to observe morphologic changes in the mediastinal lymph nodes of the rats.

were counted. Numerous genes in CNT-2-exposed cells were markedly upregulated or downregulated compared with the differences observed in CNT-1-exposed cells (Figure 9A). Significantly overrepresented GO categories among upregulated genes of CNT-1-exposed cells were classified into biological processes, namely ''sterol biosynthetic process'' (GO: 0016126; p value: 1.69×10^{-29}), ''lipid biosynthetic process'' (GO: 0008610; p value: 2.89×10^{-24}), and ''response to stimulus'' (GO: 0050896; p value: 1.71×10^{-6}). Significantly overrepresented GO categories for upregulated genes of CNT-2-exposed cells were classified into biological processes, such as ''response to external stimulus'' (GO: 0009605; p value: 4.4×10^{-51}), ''apoptotic process'' (GO: 0006915; p value: 2.61×10^{-44}), and ''lipid biosynthetic process'' (GO: 0008610; p value: 9.72×10^{-43}). The p values of the significantly overrepresented GO term ''response to stimulus'' (GO: 0050896) indicated that the expression of genes in this category was much more highly induced by CNT-2 exposure (p value: 1.80×10^{-29}) than by CNT-1 exposure (p value: 1.71×10^{-6}). Similarly, downregulated genes relevant to response to stimulus (GO: 0009605) were much more highly induced by CNT-2 exposure (p value: 2.40×10^{-13}) than by CNT-1 exposure (p value: 1.18×10^{-3}). The expression patterns of genes relevant to ''Response to stimulus'' evaluated using heat map images suggested that SWCNTs with a relatively thick bundle and long linear shapes (CNT-2) more sensitively induced cellular responses than SWCNTs with relatively thin bundles with short linear shapes (CNT-1) (Figure 9B).

Next, we compared the expression levels of genes in both *in vivo* and *in vitro* tests. Several genes involved in the response to stimulus, such as *Ccl3* (MIP-1α), *Ccl22*, *Fosl1* (encoding a protein that exhibits DNA binding), *Il1m* (encoding a protein that binds the interleukin-1 receptor), *Itgam* (encoding a protein that exhibits protein heterodimerization activity), *Serpine1* (encoding a protein that exhibits protease binding and serine-type endopeptidase inhibitor activity), *Lcn2* (encoding a member of the lipocalin superfamily with diverse functions), and *Sod2* (encoding a protein that exhibits DNA binding) were persistently upregulated through 90 d post-instillation in the high-dose CNT-1 and CNT-2 groups (Table 2). However, gene expression analysis in *in vitro* tests revealed that these genes were upregulated in CNT-2-exposed cells, but not in CNT-1-exposed cells. The chemokine (C-X-C motif) ligand *Cxcl1* (CINC-1) and *Cxcl2* (Mip-2) genes, which can act as a neutrophil chemoattractant or play a role in the acute phase of inflammatory responses, were upregulated throughout the observation period (CNT-1 group) and significantly upregulated at 1 d post-exposure (CNT-2 group) in *in vivo* tests. Considering that these were *in vitro* tests, the expression levels were remarkably high in only CNT-2-exposed cells.

Discussion

Total protein levels, neutrophil and atypical macrophage counts, and MIP-1α production in the BALF from the high-dose CNT-1 group were significantly elevated over time.

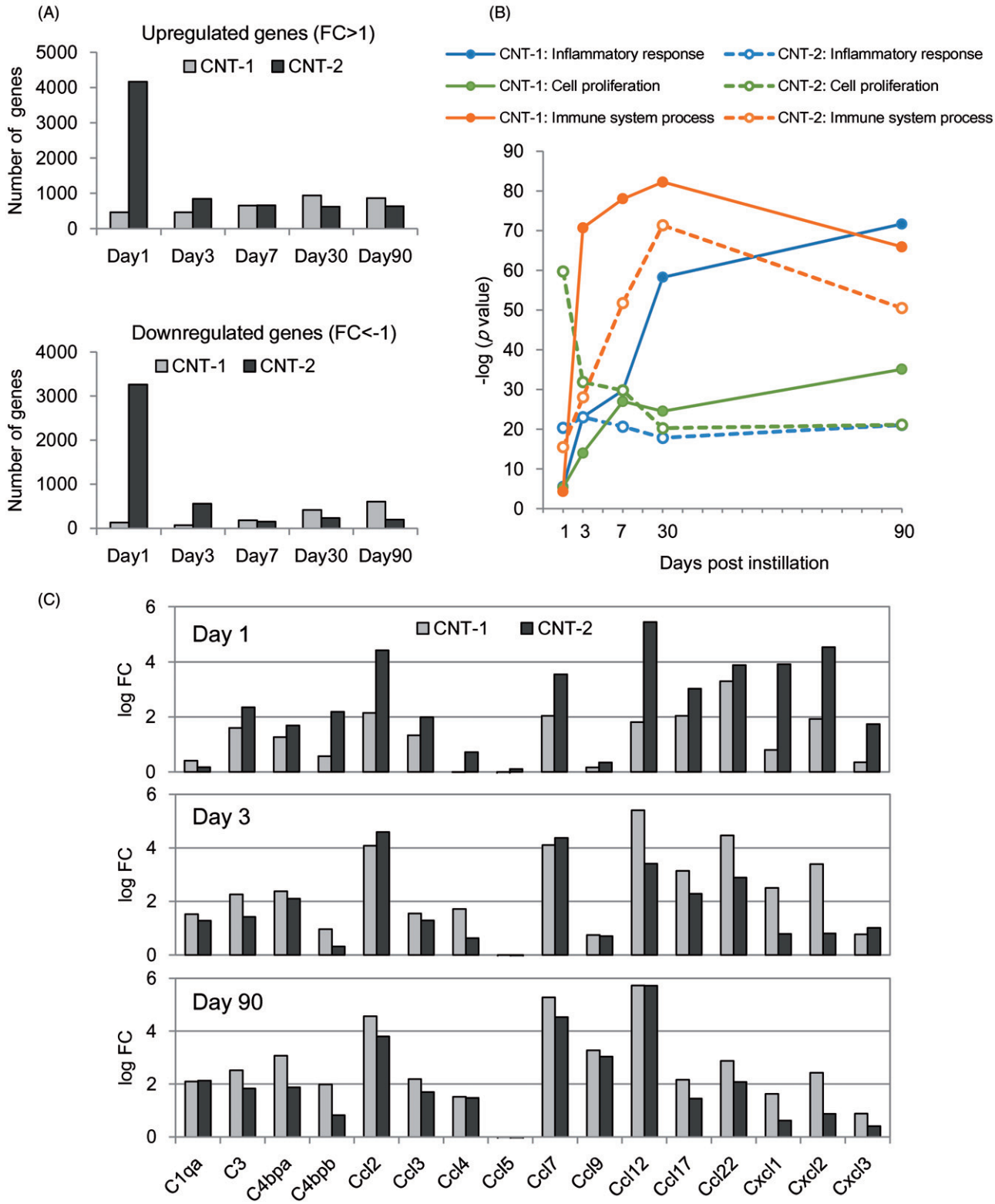

Figure 6. Changes in gene expression over time in rat lungs intratracheally instilled with CNT-1 or CNT-2 in the high-dose group. Number of significantly upregulated or downregulated genes at each time point following exposure to CNT-1 or CNT-2 (A). Changes in p values over time for the statistically overrepresented GO terms ''inflammatory response'' (GO: 0006954), ''cell proliferation'' (GO: 0008283), and ''immune system process'' (GO: 0002376) among CNT-1 and CNT-2-induced genes (FC > 1 or FC < −1) with $p < 0.05$ (B). Number of selectively upregulated genes involved in inflammatory responses at 1, 3, and 90 d post-instillation with CNT-1 or CNT-2 (C). Number of upregulated or downregulated genes with $p < 0.05$ at each time point.

In addition, neutrophils were dominant through 90 d after instillation. However, high-dose CNT-2 treatment increased the levels of total protein at 1 d post-instillation, which then decreased over time. Neutrophil, lymphocyte, and atypical macrophage counts in the BALF were elevated through 30 d after instillation and were reduced at 90 d post-instillation. The ratio of normal macrophages in BALF increased over time. These results suggest that high-dose CNT-1 exposure

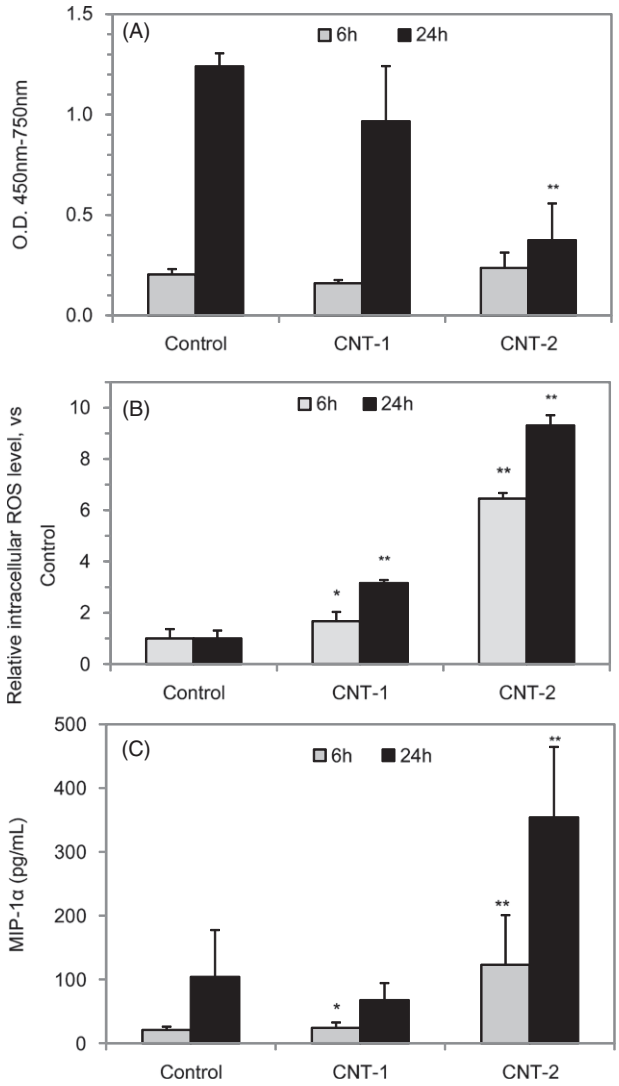

Figure 7. Effects of CNT-1 or CNT-2 on cell viability, intracellular ROS levels, and MIP-1α expression in NR8383 cells. Cell viability was measured using the WST-1 assay after exposure to CNT-1 or CNT-2 for 6 or 24 h. The viability of CNT-1- and CNT-2-treated cells in the WST-1 assay is expressed as the percentage of live cells remaining compared to that observed for untreated control cells (A). Intracellular ROS levels were measured in DCFH-DA assays with a flow cytometer following exposure to CNT-1 or CNT-2 for 6 or 24 h. DCFH-DA fluorescence in treated cells was expressed as the ratio to that observed in untreated control cells, which was set to 100% (B). The levels of MIP-1α in NR8383 cells exposed to CNT-1 or CNT-2 for 6 h or 24 h were measured. Values are the mean ± SD of four independent experiments. $^{**}p < 0.01$, $^{*}p < 0.05$ (versus control cells at each time point, Dunnett, ANOVA; C).

caused persistent inflammation during the observation period, whereas high-dose CNT-2 exposure caused acute inflammation and recovery by 90 d post-instillation.

Although the mechanisms involved in granuloma formation remain unclear, granulomas display unique histopathological signs of toxicity for SWCNTs. Several studies have reported histopathological findings of granuloma formation in rat lungs after intratracheal instillation of SWCNTs. In our previous study, persistence of alveolar macrophage-containing granulomas was observed around SWCNT aggregate sites following fibrin deposition at 90 d post-instillation at a dose of 0.4 mg per rat (Fujita et al., 2014a). Non-uniformly distributed multifocal granulomas were observed in rats intratracheally instilled with SWCNTs at 1.0 mg/kg at 1 month post-instillation (Warheit et al., 2004). Granulomas were observed in rats intratracheally instilled with highly pure SWCNTs at concentrations of 0.04 mg/kg, 0.2 mg/kg, or 1.0 mg/kg at 3 d post-instillation (Kobayashi et al., 2011). Lam et al. suggested that CNTs are capable of inducing granulomas in rodents, and their findings, together with a report from Warheit et al. (2004) are suggestive of a fundamental difference between the unique physico-chemical properties of CNTs and those of carbon black, which did not cause granuloma formation in rats. The study proposed that granulomas can impair cellular and physiological lung function, generating fibrosis, more defined nodules, and additional lesions (Lam et al., 2004). In addition, granuloma formation around the activated macrophages may play a role in protecting the surrounding host tissue from destructive chronic inflammation. Alveolar macrophages appear to initiate SWCNT-induced pathogenesis through SWCNT phagocytosis, followed by the release of various cytokines to recruit distinct immune cells and promote granuloma formation (Chou et al., 2008). The present study demonstrated that macrophage-containing granulomas developing around the sites of CNT-1 aggregates accumulated by 30 d post-instillation, whereas macrophage-containing granulomas around the sites of CNT-2 aggregates had accumulated by 3 d post-instillation. These delayed histopathological signs suggested that the size of the SWCNTs exerted different effects on lung inflammation.

Alterations in gene expression profiles have mainly been assessed in *in vitro* assays for a diverse group of nanomaterials (Dong et al., 2012). We examined the gene expression profiles of *in vivo* animal tissues or *in vitro* cell lines following exposure to ultrafine titanium dioxide particles, nickel oxides, C_{60} fullerenes, or SWCNT-containing residual metallic impurities (Fujita et al., 2009a,b, 2010, 2014a). Our studies suggested that gene expression profiling analysis can provide valuable information when comparing the effects of nanomaterials at the transcriptional level. In this study, numerous genes were strongly upregulated or downregulated by CNT-2 exposure at 1 d post-instillation, the number of which became similar to those activated in the CNT-1 groups at 3 d post-instillation. CNT-2 induced many genes involved in inflammatory responses (e.g. complement component genes and chemokines) at 1 d post-instillation. In contrast, CNT-1 significantly induced genes involved in inflammatory responses, cell proliferation, and immune system processes at 7 or 30 d post-instillation. These gene expression profiles are in agreement with the delayed total protein levels, expression of MIP-1α, cell counts in BALF analysis, and histopathological signs observed following CNT-1 and CNT-2 exposure. Thus, we propose that the relatively small SWCNT bundles with short linear shapes cause pulmonary inflammation shortly after instillation, where large SWCNT bundles with long linear shapes cause time-delayed pulmonary inflammation and slower recovery.

Gene expression analysis in this study revealed that CNT-1 induced higher gene upregulation for a 90-d period following instillation, compared with expressed genes involved in inflammatory responses and oxidative stress after intratracheal instillation with SWCNT containing residual metallic

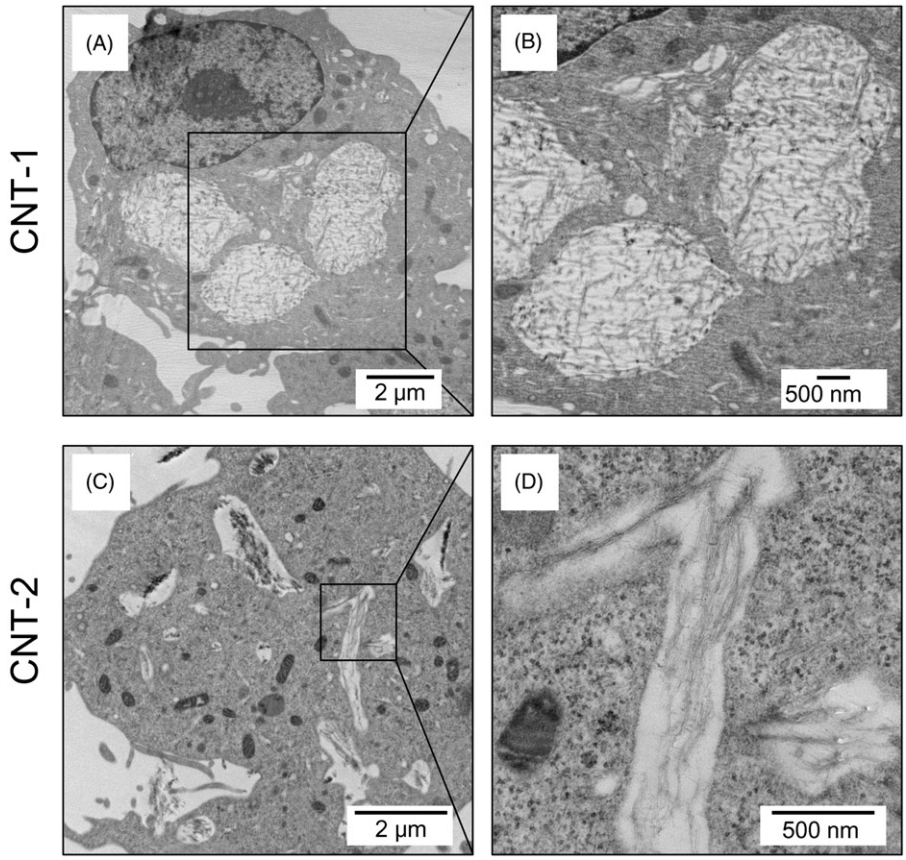

Figure 8. TEM images of NR8383 cells exposed to CNT-1 (A and B) or CNT-2 (C and D) for 24 h. Images in A and C are shown enlarged in B and D, respectively.

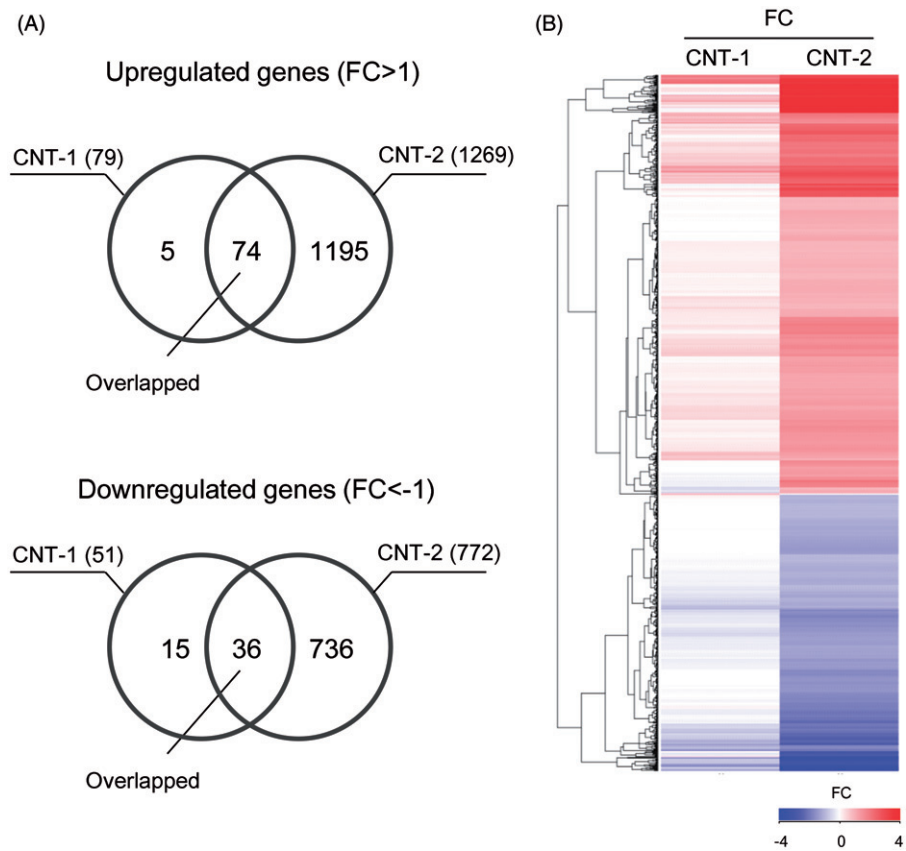

Figure 9. Effects of CNT-1 and CNT-2 on gene expression in NR8383 cells. Venn diagram showing the number of upregulated and downregulated genes in NR8383 cells exposed to CNT-1 or CNT-2 for 24 h (A). Heat map generated from DNA microarray data reflecting differential expression of genes involved in the response to stimulus (GO: 0050896) in NR8383 cells exposed to CNT-1 or CNT-2 for 24 h. Expression levels are colored blue for low intensity and red for high intensity (see scale at the bottom right corner) (B).

Table 2. Selected list of rat genes involved in the response to stimulus that were up-regulated following exposure to CNT-1 or CNT-2 in *in vivo* and *in vitro*.

		CNT-1						CNT-2						
		In vivo test*						*In vivo* test*						
GeneBank Accession No.	Gene name	Day 1	Day 3	Day 7	Day 30	Day 90	*in vitro* test	Day 1	Day 3	Day 7	Day 30	Day 90	*in vitro* test	Description
NM_017134	*Arg1*	0.3	**1.1**	**1.5**	**2.0**	**1.8**	**0.3**	**2.7**	**1.7**	0.9	**1.5**	**1.1**	**4.2**	Arginase 1
NM_016995	*C4bpb*	0.6	**1.0**	**1.4**	**1.5**	**2.0**	0.9	**2.2**	0.3	**1.0**	1.0	**0.8**	1.5	Complement component 4 binding protein, beta
NM_013025	*Ccl3*	**1.3**	**1.6**	**2.0**	**2.2**	**2.2**	**0.9**	**2.0**	**1.3**	**2.1**	**1.8**	**1.7**	**2.2**	Chemokine (C-C motif) ligand 3
NM_057203	*Ccl22*	**3.3**	**4.5**	**2.6**	**2.6**	**2.9**	0.1	**3.9**	**2.9**	**1.7**	**2.1**	**2.1**	**1.2**	Chemokine (C-C motif) ligand 22
NM_030845	*Cxcl1*	0.8	**2.5**	**1.3**	**1.5**	**1.6**	**1.1**	**3.9**	0.8	**0.9**	**1.1**	**0.6**	**4.5**	Chemokine (C-X-C motif) ligand 1
NM_053647	*Cxcl2*	**1.9**	**3.4**	**2.7**	**2.1**	**2.4**	0.6	**4.5**	0.8	**1.2**	**1.0**	**0.9**	**6.3**	Chemokine (C-X-C motif) ligand 2
NM_012953	*Fosl1*	**2.6**	**2.3**	**2.4**	**2.8**	**2.9**	0.6	**5.2**	**2.7**	**2.3**	**1.5**	**1.5**	**4.9**	Fos-like antigen 1
NM_022194	*Il1rn*	**1.1**	**1.6**	**2.4**	**2.9**	**2.8**	−0.1	**2.1**	**2.4**	**1.8**	**2.1**	**1.9**	**2.9**	Interleukin 1 receptor antagonist
NM_012711	*Itgam*	**2.1**	**2.0**	**3.1**	**3.7**	**3.4**	**1.0**	**1.5**	**3.5**	**3.7**	**3.1**	**3.1**	**3.5**	Integrin, alpha M
NM_012620	*Serpine1*	**1.7**	**3.2**	**3.1**	**3.0**	**2.5**	−0.2	**2.6**	**4.1**	**3.4**	**2.8**	**2.5**	**2.1**	Serpin peptidase inhibitor, clade E, member 1
NM_130741	*Lcn2*	**2.8**	**4.6**	**4.7**	**4.1**	**4.1**	**0.5**	**4.1**	**2.8**	**3.3**	**3.4**	**3.1**	**3.7**	Lipocalin 2
NM_012580	*Hmox1*	−0.1	1.0	**1.2**	**1.7**	**2.3**	**0.6**	**−2.4**	1.7	**1.6**	**1.6**	**1.9**	**1.6**	Heme oxygenase (decycling) 1
NM_017051	*Sod2*	**2.3**	**2.3**	**1.9**	**2.4**	**2.7**	**0.6**	**3.1**	**1.5**	**1.3**	**1.7**	**1.5**	**1.7**	Superoxide dismutase 2, mitochondrial
NM_053963	*Mmp12*	**3.5**	**4.3**	**4.6**	**5.9**	**6.3**	**0.6**	**3.3**	**7.0**	**7.2**	**6.3**	**6.2**	**3.9**	Matrix metallopeptidase 12
NM_012864	*Mmp7*	**3.7**	**4.8**	**7.8**	**8.2**	**7.4**	0.2	**5.5**	**8.7**	**9.6**	**8.5**	**7.8**	**−2.0**	Matrix metallopeptidase 7
NM_012881	*Spp1*	**4.8**	**5.1**	**7.9**	**8.6**	**8.8**	0.6	**6.9**	**10.6**	**9.8**	**8.0**	**8.0**	**4.2**	Secreted phosphoprotein 1

*Samples in high dose groups were evaluated.

Numerical values represent log-fold gene expression changes relative to control levels. Log-fold changes with *p* values less or equal than 0.05 are shown in bold.

impurities (Fujita et al., 2014a). The length (0.51 μm) and the dose (0.4 mg/rat) of the impurity-free SWCNTs used in this study were similar to those of SWCNTs, except that they contained residual metallic impurities (0.69 μm and 0.4 mg/rat) (Morimoto et al., 2012). Taken together with previous histopathological examinations and BALF analyses, our findings indicate that the impurity-free SWCNTs used in this study exert higher pulmonary toxicity than SWCNTs containing residual metallic impurities.

It has been reported that MWCNTs penetrate the pleura after pharyngeal aspiration of MWCNTs (Mercer et al., 2011; Porter et al., 2013). Deposition of MWCNTs was observed in the posterior mediastinal lymph node of rats intratracheally instilled with MWCNTs, at 91 d post-instillation (Aiso et al., 2011). MWCNTs were identified in the deep paracortical region of lymph nodes in MWCNT-exposed mice (10 mg/m^3, 5 h/d) after 8 and 12 d of exposure, suggesting that MWCNTs were translocated from the lungs to the tracheobronchial lymph nodes in mice (Porter et al., 2010). Results from a study examining the intrapleural administration of carbon nanotubes suggested that short fibers and small CNT tangles that deposit in alveoli were situated subpleurally, migrated to the pleural space, and exited in the flow of pleural fluid through the stomata, where they followed the lymphatic drainage to the mediastinal lymph nodes. Long fibers and long CNTs also reach the pleural space from subpleural alveoli, but they cannot negotiate the stomata and are retained, where they cause inflammation and potentially long-term disease (Murphy et al., 2011). In this study, we identified SWCNTs in the mediastinal lymph nodes in high-dose CNT-1 and CNT-2 groups at 90 d post-instillation. To our knowledge, this is the first direct evidence showing the translocation of SWCNTs from the lungs. Our results showed that SWCNTs, regardless of their size, are most likely to penetrate the pleura after intratracheal instillation and to translocate to the mediastinal lymph nodes. However, the size-dependent retention and impact of SWCNTs in the pleural space of the lungs are still unclear.

Intracellular SWCNTs were observed in CNT-1 or CNT-2–treated cells over a short exposure period by TEM, and the data showed that the cells maintained their physical structures. In such situations, it is of interest that the cell viability, intracellular ROS production, release of cytokines, and gene expression profiles between CNT-1 and CNT-2 varied. The WST-1-based viability assay demonstrated that CNT-2 had little effect on cell viability after 24 h of exposure. Intracellular ROS production was induced by CNT-1 and CNT-2. ROS levels in CNT-2-treated samples were higher than those in CNT-1-treated samples. CNT-2 treatment evoked the release of the inflammatory cytokine MIP-1α, whereas CNT-1 did not induce cytokine production. The expression of several representative genes involved in the response to stimulus (e.g. *Arg1*, *C4bpb*, *Ccl3*, *Ccl22*, *Cxcl1*, *Cxcl2*, *Fosl1*, *Il1rn*, *Itgam*, *Serpine1*, *Lcn2*, *Hmox1*, *Sod2*, *Mmp12*, and *Spp1* genes) was markedly increased in NR8383 cells exposed to CNT-2 compared with cells exposed to CNT-1. Our previous study suggested that the physical properties of SWCNTs, especially the size and the length of SWCNT

bundles, when dispersed in cell culture medium influenced ROS generation in A549 cells, even with the same bulk SWCNTs (Fujita et al., 2013). The results of this study thus suggest that SWCNTs assembled into relatively thick bundles with a long, linear shape elicit potent cellular responses in rat alveolar macrophages, compared with SWCNTs assembled into relatively thin bundles with a short, linear shape.

The mechanism of intracellular ROS generation by SWCNTs exposure is still unclear. It has been proposed that the residual catalytic metals in SWCNTs contribute to the induction of oxidative stress (Kagan et al., 2006; Shvedova et al., 2003). In particular, the role of iron is important for oxidative reactions. A Fenton-like reaction may play a role in the generation of hydroxyl radicals in SWCNT-stimulated HaCaT cells (Shvedova et al., 2003). The manufacture of SWCNTs depends on the use of catalytic metals, e.g. Fe, Co, and Ni, which are known to induce ROS formation and subsequently cause oxidative stress (Chachami et al., 2004; Sharma et al., 2007; Shvedova & Kagan, 2010). In contrast, our latest study supports the conclusion that the iron involved in the manufacture of the SWCNTs may not be a definitive parameter for intracellular ROS production in A549 cells (Fujita et al., 2013). In this study, ICP-MS analysis revealed that the metal content of CNT-1 and CNT-2 was undetectable, confirming that these nanotubes were derived from the impurity-free carbon materials. However, ROS production was determined in cells treated with CNT-1 and CNT-2. These results suggest that our hypothesis, which states that residual metallic impurities are not a key determinant of SWCNT-mediated ROS production, would be applicable not only to alveolar epithelial cells but also to alveolar macrophages.

It is important to relate *in vitro* studies with *in vivo* studies when considering the influence of SWCNTs on human health. In a recent study, it was proposed that the activity of MWCNTs in an optimized *in vitro* proliferation assay using MLg cells strongly reflects lung fibrosis potential *in vivo* (Vietti et al., 2013). *In vitro* cell-based assays are advantageous in that they can provide a simple model to understand the mechanisms of cytotoxicity. However, it is often pointed out that *in vitro* results often lack correlation with *in vivo* toxicological studies. It is not easy for *in vitro* studies to validate the subchronic or chronic *in vivo* toxic assessment following exposure. Overall, this *in vivo* study revealed that CNT-2 was influential immediately after instillation; however, CNT-1 exerted an inflammogenic impact after at 3 or 7 d post-instillation. Compared with the gene expression profiles in this study, many genes involved in the response to stimulus at day 1 post-instillation were upregulated *in vitro* by CNT-2. However, CNT-1 tended not to show an association between *in vivo* and *in vitro* results. Thus, these results suggested that rat alveolar macrophage NR8383 cells were useful to evaluate acute *in vivo* toxic assessment following exposure. We propose that SWCNTs with a relatively thick bundle and long linear shapes sensitively induce cellular responses in alveolar macrophages and elicit acute lung inflammation shortly after inhalation; in contrast, SWCNTs formed as relatively thin bundles with short linear shapes elicit pulmonary inflammation with slower recovery. Thus, we conclude that the pulmonary toxicity of SWCNTs is closely associated with the size and length of the bundles.

Acknowledgements

The authors would like to thank Ms. Emiko Kobayashi at the National Institute of Advanced Industrial Science and Technology (AIST) for help in performing the TEM analysis. This study is based on the results obtained for the project ''Innovative carbon nanotubes composite materials project toward achieving a low-carbon society (P10024)'' commissioned by the New Energy and Industrial Technology Development Organization (NEDO), Japan.

Declaration of interest

The authors report that they have no conflicts of interest.

References

Aiso S, Kubota H, Umeda Y, et al. (2011). Translocation of intratracheally instilled multiwall carbon nanotubes to lung-associated lymph nodes in rats. Ind Health 49:215–20.

Beissbarth T, Speed TP. (2004). GOstat: find statistically overrepresented gene ontologies within a group of genes. Bioinformatics 20: 1464–5.

Brown DM, Kinloch IA, Bangert U, et al. (2007). An *in vitro* study of the potential of carbon nanotubes and nanofibres to induce inflammatory mediators and frustrated phagocytosis. Carbon 45:1743–56.

Chachami G, Simos G, Hatziefthimiou A, et al. (2004). Cobalt induces hypoxia-inducible factor-1 alpha expression in airway smooth muscle cells by a reactive oxygen species- and PI3K-dependent mechanism. Am J Respir Cell Mol Biol 31:544–51.

Chou CC, Hsiao HY, Hong QS, et al. (2008). Single-walled carbon nanotubes can induce pulmonary injury in mouse model. Nano Lett 8: 437–45.

Davoren M, Herzog E, Casey A, et al. (2007). *In vitro* toxicity evaluation of single walled carbon nanotubes on human A549 lung cells. Toxicol *In Vitro* 21:438–48.

Donaldson K, Murphy FA, Duffin R, Poland CA. (2010). Asbestos, carbon nanotubes and the pleural mesothelium: a review of the hypothesis regarding the role of long fibre retention in the parietal pleura, inflammation and mesothelioma. Part Fibre Toxicol 7:5.

Donaldson K, Poland CA, Murphy FA, et al. (2013). Pulmonary toxicity of carbon nanotubes and asbestos – similarities and differences. Adv Drug Deliv Rev 65:2078–86.

Dong PX, Wan B, Guo LH. (2012). *In vitro* toxicity of acid-functionalized single-walled carbon nanotubes: effects on murine macrophages and gene expression profiling. Nanotoxicology 6: 288–303.

Elgrabli D, Abella-Gallart S, Aguerre-Chariol O, et al. (2007). Effect of BSA on carbon nanotube dispersion for *in vivo* and *in vitro* studies. Nanotoxicology 1:266–78.

Fujita K, Fukuda M, Endoh S, et al. (2013). Physical properties of single-wall carbon nanotubes in cell culture and their dispersal due to alveolar epithelial cell response. Toxicol Mech Methods 23:598–609.

Fujita K, Fukuda M, Fukui H, et al. (2014a). Intratracheal instillation of single-wall carbon nanotubes in the rat lung induces time-dependent changes in gene expression. Nanotoxicology:1–12.

Fujita K, Endoh S, Maru J, et al. (2014b). Sample preparation and characterization for safety testing of carbon nanotubes, and *in vitro* cell-based assay. Available from: http://en.aist-riss.jp/assessment/2571/. [Last accessed: on 31 Mar 2014].

Fujita K, Horie M, Kato H, et al. (2009a). Effects of ultrafine TiO_2 particles on gene expression profile in human keratinocytes without illumination: involvement of extracellular matrix and cell adhesion. Toxicol Lett 191:109–17.

Fujita K, Morimoto Y, Endoh S, et al. (2010). Identification of potential biomarkers from gene expression profiles in rat lungs intratracheally instilled with C(60) fullerenes. Toxicology 274:34–41.

Fujita K, Morimoto Y, Ogami A, et al. (2009b). Gene expression profiles in rat lung after inhalation exposure to C60 fullerene particles. Toxicology 258:47–55.

Gernand JM, Casman EA. (2014). A meta-analysis of carbon nanotube pulmonary toxicity studies – how physical dimensions and impurities affect the toxicity of carbon nanotubes. Risk Anal 34:583–97.

Hata K, Futaba DN, Mizuno K, et al. (2004). Water-assisted highly efficient synthesis of impurity-free single-waited carbon nanotubes. Science 306:1362–4.

Herzog E, Byrne HJ, Casey A, et al. (2009). SWCNT suppress inflammatory mediator responses in human lung epithelium *in vitro*. Toxicol Appl Pharmacol 234:378–90.

Horie M, Fujita K. (2011). Chapter four-toxicity of metal oxides nanoparticles. In: James CF, (ed). Advances in molecular toxicology, vol. 5. Oxford: Elsevier, 145–78.

Horie M, Kato H, Fujita K, et al. (2012). *In vitro* evaluation of cellular response induced by manufactured nanoparticles. Chem Res Toxicol 25:605–19.

Horie M, Nishio K, Fujita K, et al. (2009). Protein adsorption of ultrafine metal oxide and its influence on cytotoxicity toward cultured cells. Chem Res Toxicol 22:543–53.

Horie M, Stowe M, Tabei M, et al. (2013). Dispersant affects the cellular influences of single-wall carbon nanotube: the role of CNT as carrier of dispersants. Toxicol Mech Methods 23:315–22.

Kagan VE, Tyurina YY, Tyurin VA, et al. (2006). Direct and indirect effects of single walled carbon nanotubes on RAW 264.7 macrophages: role of iron. Toxicol Lett 165:88–100.

Kato H, Suzuki M, Fujita K, et al. (2009). Reliable size determination of nanoparticles using dynamic light scattering method for *in vitro* toxicology assessment. Toxicol *In Vitro* 23:927–34.

Kobayashi N, Naya M, Mizuno K, et al. (2011). Pulmonary and systemic responses of highly pure and well-dispersed single-wall carbon nanotubes after intratracheal instillation in rats. Inhal Toxicol 23: 814–28.

Lam CW, James JT, McCluskey R, Hunter RL. (2004). Pulmonary toxicity of single-wall carbon nanotubes in mice 7 and 90 days after intratracheal instillation. Toxicol Sci 77:126–34.

Manna SK, Sarkar S, Barr J, et al. (2005). Single-walled carbon nanotube induces oxidative stress and activates nuclear transcription factor-kappa B in human keratinocytes. Nano Lett 5: 1676–84.

Mercer RR, Hubbs AF, Scabilloni JF, et al. (2011). Pulmonary fibrotic response to aspiration of multi-walled carbon nanotubes. Part Fibre Toxicol 8:21.

Morimoto Y, Hirohashi M, Horie M, et al. (2012). Pulmonary toxicity of well-dispersed single-wall carbon nanotubes following intratracheal instillation. J Nano Res 18–19:9–25.

Murphy FA, Poland CA, Duffin R, et al. (2011). Length-dependent retention of carbon nanotubes in the pleural space of mice initiates sustained inflammation and progressive fibrosis on the parietal pleura. Am J Pathol 178:2587–600.

Mutlu GM, Budinger GR, Green AA, et al. (2010). Biocompatible nanoscale dispersion of single-walled carbon nanotubes minimizes *in vivo* pulmonary toxicity. Nano Lett 10:1664–70.

Poland CA, Duffin R, Kinloch I, et al. (2008). Carbon nanotubes introduced into the abdominal cavity of mice show asbestos-like pathogenicity in a pilot study. Nat Nanotechnol 3:423–8.

Porter DW, Hubbs AF, Chen BT, et al. (2013). Acute pulmonary dose-responses to inhaled multi-walled carbon nanotubes. Nanotoxicology 7:1179–94.

Porter DW, Hubbs AF, Mercer RR, et al. (2010). Mouse pulmonary dose- and time course-responses induced by exposure to multi-walled carbon nanotubes. Toxicology 269:136–47.

Pulskamp K, Diabate S, Krug HF. (2007). Carbon nanotubes show no sign of acute toxicity but induce intracellular reactive oxygen species in dependence on contaminants. Toxicol Lett 168:58–74.

Sharma CS, Sarkar S, Periyakaruppan A, et al. (2007). Single-walled carbon nanotubes induces oxidative stress in rat lung epithelial cells. J Nanosci Nanotechnol 7:2466–72.

Shvedova AA, Castranova V, Kisin ER, et al. (2003). Exposure to carbon nanotube material: assessment of nanotube cytotoxicity using human keratinocyte cells. J Toxicol Environ Health A 66:1909–26.

Shvedova AA, Kagan VE. (2010). The role of nanotoxicology in realizing the 'helping without harm' paradigm of nanomedicine: lessons from studies of pulmonary effects of single-walled carbon nanotubes. J Intern Med 267:106–18.

Vietti G, Ibouraadaten S, Palmai-Pallag M, et al. (2013). Towards predicting the lung fibrogenic activity of nanomaterials: experimental validation of an *in vitro* fibroblast proliferation assay. Part Fibre Toxicol 10:52.

Wang L, Castranova V, Mishra A, et al. (2010). Dispersion of single-walled carbon nanotubes by a natural lung surfactant for pulmonary *in vitro* and *in vivo* toxicity studies. Part Fibre Toxicol 7:31.

Warheit DB, Laurence BR, Reed KL, et al. (2004). Comparative pulmonary toxicity assessment of single-wall carbon nanotubes in rats. Toxicol Sci 77:117–25.

Worle-Knirsch JM, Pulskamp K, Krug HF. (2006). Oops they did it again! Carbon nanotubes hoax scientists in viability assays. Nano Lett 6:1261–8.